# Design, component selection and critical considerations for the development of a 50 kWe Carnot Battery coupled to waste heat

Aitor Cendoya[1]*, Frederic Ransy[1], Olivier Dumont[1], Bentao Guo[1], Vincent Lemort[1]

[1] *Thermodynamics Laboratory, Faculty of Applied Sciences, University of Liege, Allée de la découverte 17, B4000 Liege-Belgium*

*Corresponding Author: acendoya@uliege.be

## ABSTRACT

Carnot Batteries (CB) integrate two conversion cycles: a power-to-heat cycle via a Heat Pump (HP) and a heat-to-power cycle using an Organic Rankine Cycle (ORC). HPs are widely available and highly efficient due to their Coefficient of Performance, while ORCs, though commercially established, exhibit low efficiency at temperatures below 120°C and require further advancements. CBs have been extensively studied in various applications. The primary barriers include high initial investment and operational complexity. Systems capable of sharing key components between HP and ORC emerge as a suitable and scalable solution, as they can significantly reduce investment costs. This paper presents the design, component selection, and key considerations for a 50 kWe and 600 kWth CB, utilising waste heat from abandoned underground caverns in southern Belgium. The system is built from off-the-shelf components, including twin-screw machines (compressor and expander), brazed plate heat exchangers, a low Net Positive Suction Head (NPSH) centrifugal pump, a liquid receiver, an expansion valve, piping, and auxiliary elements. The study addresses 3D design, structural considerations, expected efficiency, and integration challenges. Through numerical simulation, it is estimated that under operating conditions, the ORC can achieve a maximum efficiency of 7.6%, and the HP a maximum Coefficient Of Performance (COP) of 6.6. Additionally, it provides critical insights into the integration of HP and ORC, highlighting control variables for optimisation. Finally, a conceptual design of the proposed machine is outlined, offering a foundation for further research and development.

## 1 INTRODUCTION

The urgent need to develop technologies that support the transition to a renewable energy-based grid is one of the greatest challenges of the century and a major global concern. Energy storage plays a crucial role in balancing Renewable Energy Source (RES) electricity production with end-user demand by absorbing excess energy from the grid and releasing it when clean energy generation declines due to its inherent intermittency and variability (Vecchi et al., 2022). One technology which has gained a lot of attraction in the past years corresponds to the Carnot Battery (CB), which consists of two main subsystems: a power-to-heat conversion unit and a heat-to-power conversion unit. One particularly promising configuration integrates low-temperature waste heat <200°C can be considered vast worldwide (Xu et al., 2019). In this type of system, due to the operating temperature levels, a refrigeration cycle is normally used to produce and generate energy. During charging, a heat pump cycle is used to thermally boost the waste heat temperature, and during discharging, an organic Rankine cycle (ORC) is used to generate electricity. The duration of storage can vary from a few tens of minutes to several weeks, depending on operating conditions, storage medium and size.

Despite its potential, CB technology faces critical challenges, particularly high investment costs, which could be reduced by implementing reversible system configurations (Daniarta et al., 2024). Research has explored CB prototypes for applications in geothermal energy (Kaufmann et al., 2024), zeotropic mixtures (Weitzer et al., 2024), building integration (Dumont, 2017), and phase change materials (Theologou et al., 2024). Despite all these prototypes developed, significant shortcomings remain.

There is a large gap for improvement in component selection and critical points to consider. In addition, this type of system can be integrated into different applications, such as operating in areas with an unstable grid (Guo et al., 2025), improving the performance of geothermal plants, and recovering part of the waste heat from the brine injection circuit, to cover auxiliary demands (Cendoya et al., 2024). Likewise, these technologies have attracted great interest in being coupled with district heat networks and multi-energy systems, dispatching heat, cooling and electricity (Cendoya et al., 2024), which also presented the possibility of participating in energy arbitrage markets and in grid frequency restoration.

Consequently, the maturity level of CB technology is still evolving, and its potential for diverse applications remains significant. Numerous ongoing projects worldwide are working to establish a robust foundation for their advancement, systematically identifying key challenges and exploring viable solutions. This article presents the design principles, essential considerations, and critical challenges involved in developing a 50 kWe and 500 kWth CB within the framework of the WeForming project. By providing a comprehensive overview, this work aims to serve as a reference for future research and contribute to the foundational development of CB technology.

## 2 CASE STUDY

In past decades, several mines across Europe have been decommissioned as they became increasingly unprofitable and were closed and abandoned. Nowadays, several of them are flooded, presenting an interesting opportunity for large-scale thermal energy storage. The demonstrator where the CB will be installed corresponds to an abandoned slate mine with a storage capacity of 500000 m$^3$. This mine is located in the town of Martelange, on the southern border between Belgium and Luxembourg. The schematic of the case study is depicted in Figure 1, which represents the facility under development, expected to be completed in early 2026. The study site includes multiple storage options:

- Low-temperature storage, 10–20°C (Cav. 1): A 20000 m³ underground volume, where the ORC condenser will reject the heat. In parallel, this heat will then be released into the medium and is not expected to overheat the cold sink.
- Medium-low-temperature storage, 25–45°C (Cav. 2): A 6000 m³ underground volume, coupled to a fourth-generation district heating network to cover the heat demand of existing buildings.
- Medium-high-temperature storage, 40–60°C (Cav. 3): A 600 m³ underground volume, which represents the waste heat integration in the CB operation.
- High-temperature storage, 80-110°C (Sto. 1): A 20 m³ insulated overground water tank, designated for storing the high-temperature energy required for ORC evaporator operation.

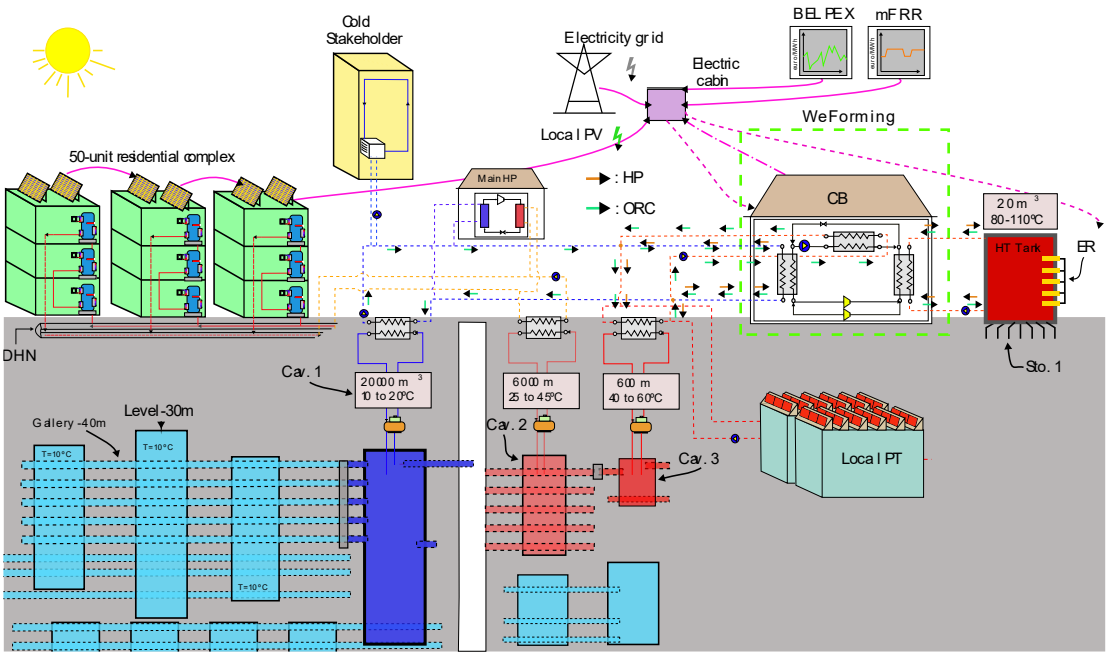


**Figure 1:** Schema of the demonstrator where the CB be installed

In addition, the installation has 70 kWe of photovoltaic (PV) panels and 140 kWth of thermal panels (PT). The PVs are used directly by the main HP to produce heat, which will then be distributed by a DHN to a building complex consisting of 50 apartments. The heat produced by the PTs is directly stored in the Cav. 3 to then feed the CB-ORC pre-heater or the CB-HP evaporator. This storage represent the potential of low-temperature waste heat, which can be replaced in another case study by available waste heat. Simultaneously, these different temperature reservoirs can exchange heat with each other. Furthermore, the demonstrator will also be interconnected with the electricity grid, consuming the surpluses from the RES, which have low or even negative prices. Whereas electricity will be produced when electricity prices reach high values. In addition, the frequency grid restoration services will be validated through the installation to see to what degree the CB can provide a reliable service.

## 3 P&ID DIAGRAMS

Figure 2 shows the P&ID of the CB to be developed, highlighting its most significant components, such as the expander, compressor, pumps, valves, sensors, the liquid tank and the different circuits. The main names of the models with their respective abbreviations in the P&ID are presented in Table 1, these are described further in the next section. The different circuits shown correspond to refrigerant (black lines) and water circuits. Between the two figures, it is possible to analyse the configuration in both modes. The different water circuits correspond to: circuit 1, connected to Sto.1, circuit 2, coming from Cav.3, and circuit 3 connected to Cav.1. Note that the oil circuit is not necessary due to the reliability of the compressor and expander, which have independent internal lubrication systems, eliminating the need for an integrated oil circuit (this is discussed in more detail below).

**Table 1:** Main components and their abbreviations in P&ID diagrams

| Abbreviation | Model | Abbreviation | Model |
|---|---|---|---|
| HX 1 | CBH210-170AH | EXP-V | 8028 / 025VDG101M |
| W1-PUMP | Etabloc 065-050 | R-PUMP | ICP2/32-185 |
| EXP | HSEL8591-110Y-40 | LIQ | RICEV. FL 40.27+SGR7+2S89 (M54/M54) |
| CP | CSH2T9573-240Y-35D | | |
| W2-PUMP | Etabloc 065-050 | HX 3 | CBH210-60AH |
| HX 2 | CB410-200M | W3-PUMP | Etabloc 065-050 |

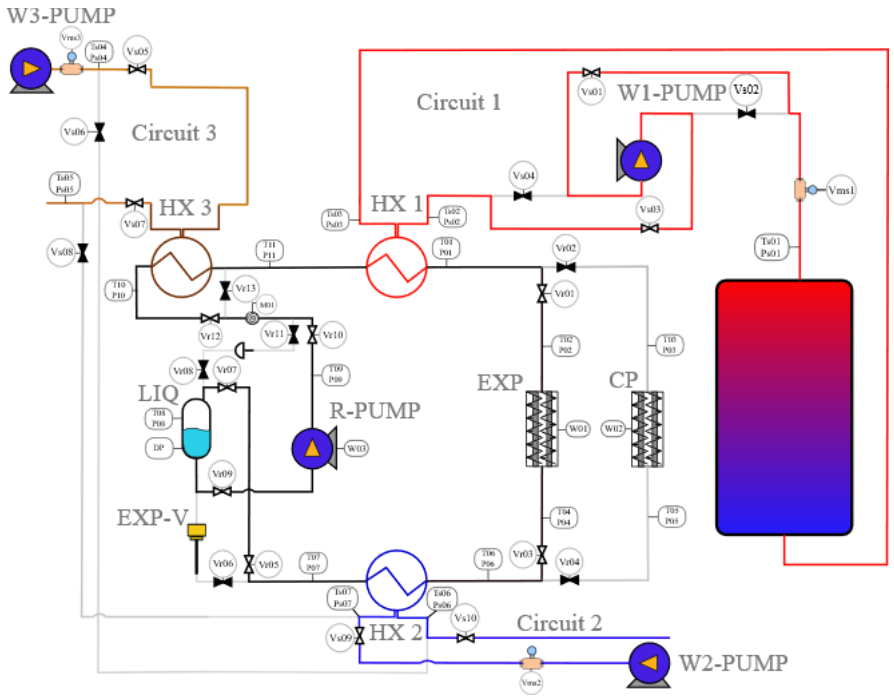


(a)

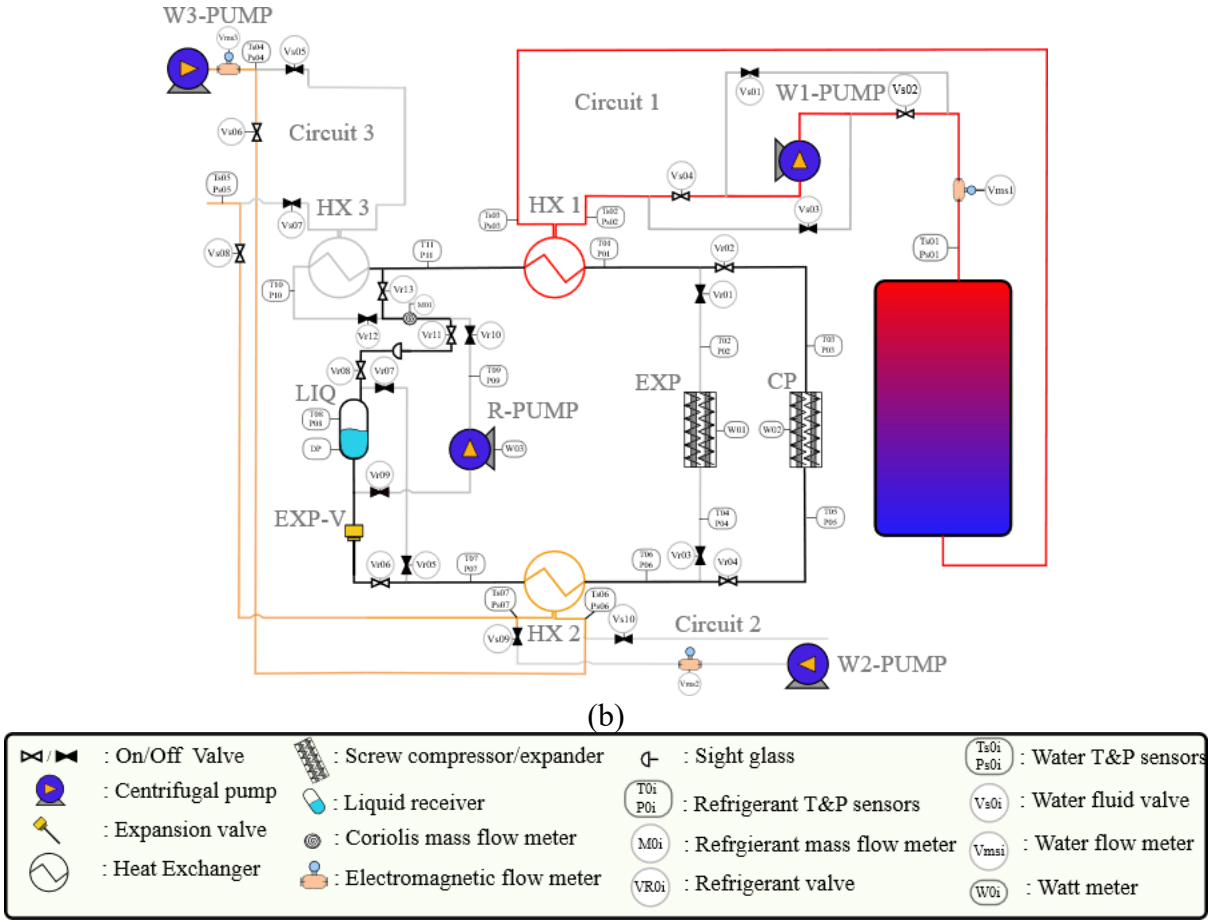


**Figure 2:** P&ID of the CB, a) ORC mode, b) HP mode and c) instrumentation and control labels

Both circuits are designed to be fully reversible, allowing shared use of sensors and valves across operational modes. Mode switching is achieved via pneumatic ball valves, which are actuated by compressed air directed to the valve head. Depending on the predefined configuration, the air pressure causes the valve to open or close. Pneumatic actuation was selected due to its substantially lower cost compared to electrically operated valves for the required diameters.

Multiple sensors are required throughout the prototype to allow effective monitoring and precise control of key operating variables, including temperature, pressure, and mass flow rates. For the refrigerant and water circuits, four Class A PT100 sensors were used per circuit, while the remaining temperature measurements were made using type T thermocouples. Table 2 details the sensor models used, along with their respective accuracies.

**Table 2:** Main components and their abbreviations in P&ID diagrams

| Sensor | Description | Model | Manufacturer | Accuracy |
|---|---|---|---|---|
| Refrigerant mass flow rate (M01) | Coriolis mass flow meter | Optimass MFS 1000 25 | Krohne | ±0.5% |
| Water volume flow rate (Vms1, Vms2 and Vms3) | Magnetic flow meters | OPTIFLUX 4000, and OPTIFLUX 2000 | Krohne | ±3% |
| Differential pressure (DP) | Refrigerant level in the tank | Rosemount Coplanar Transmitter | Emerson | ±0.025% |

| | | | | |
|---|---|---|---|---|
| Pressure sensors refrigerant (low pressure) | Flush pressure sensor | PM1515 | IFM | ± 0.1% |
| Pressure sensors refrigerant (high pressure) | Flush pressure sensor | PM1514 | IFM | ± 0.1% |
| Pressure sensors water | Flush pressure sensor | PM1515 | IFM | ± 0.1% |
| Temperature sensors | PT100 Class A | TM4511 | IFM | ± 0.15 K |

## 4 SELECTION OF COMPONENTS

The requirements of the CB are defined in the framework of the WeForming project, where the system must generate 50 kWe in the ORC mode and 600 kWth in the HP mode. The operating temperature limitations are mainly dictated by underground caverns. Specifically, the submersible pumps are not designed to operate at temperatures above 60 °C. However, technological advances or the application of motor cooling strategies may allow higher temperatures to be reached. The nominal operating conditions differ in two modes. In ORC mode, the water supply temperatures are condenser: 15°C (Cav. 1), preheater: 50°C (Cav. 3) and evaporator: 100°C (Sto.1). In HP mode, the water supply temperatures are condenser: 95°C (Sto. 1) and evaporator: 50°C (Cav.3).

Two independent volumetric machines were used to optimise performance in each mode, as a single unit limited the operating range and introduced complexity into the design, such as the oil circuit, which would have had to be completely replaced. Additionally, the expander operates with a unidirectional energy flow from the generator to the grid, which restricts operation in the other direction (reversible) (Weitzer et al., 2023). Moreover, to reduce inertia between modes, aiming to provide flexible services to the grid, the machines were separated. Suitable candidates for supplying an expander of this power are very limited. Therefore, the semi-hermetic twin-screw expander HSEL8591-110Y-40 (displacement of 251 $m^3/h$ at 50 Hz) from Bitzer has been chosen, which at 50 Hz can produce a maximum power of 77 kWe, which is one of the best choices for the operating powers (Dumont et al., 2018). The selected compressor must be able to reach a refrigerant saturation temperature in the condenser of up to 125°C and achieve the desired heat output. For this purpose, the Bitzer compact twin-screw compressor CSH2T9573-240Y-35D (displacement of 845 $m^3/h$ at 60 Hz) is also chosen due to its higher efficiency and high reliability. Brazed Plate heat exchangers are selected to be shared in both modes due to the high performance in liquid-liquid heat exchange at low and medium-low pressure. Models CB410-200M ($\dot{Q}_{nom} = 549.7\ kW, A = 74.6\ m^2$), CBH210-170AH ($\dot{Q}_{nom} = 389.6\ kW, A = 42.34\ m^2$) and CB210-60 ($\dot{Q}_{nom} = 210.8\ kW, A = 14.62\ m^2$), from manufacturer Alfa Laval, correspond to the condenser, evaporator and preheater, respectively, in ORC mode, while CB410-200M and CBH210-170AH correspond to the evaporator and condenser in HP mode.

The prototype will be transported from the Thermodynamics Laboratory of the University of Liege to the demonstration site. For this purpose, a 20-foot flat rack container has been chosen as part of the CB machine. In this respect, the available head is limited to the height of the container due to transportation regulation limitations. This leads to restrictions in pump operation, whereby a very low NPSH pump is required. Centrifugal pumps are preferred over other pumps because of their higher efficiency (Dumont, 2017). A Verder Low-NPSH centrifugal pump (ICP2/32-185) for ORC mode was selected for this process. In order to avoid overheating problems in the expansion valve, which have already been reported (Ravindran et al., 2024) when working at high temperatures in HPs, a pneumatic valve 8028 / 025VDG101M from the manufacturer Shulbert & Salzer, controlled via a 4-20 mA analogue input, is chosen, model 8401-4. This valve prevents overheating problems in the controller due to the distance between it and the valve in contact with the refrigerant. At the same time, it allows the fluid to be regulated precisely and by means of instantaneous changes. Furthermore, to achieve highly efficient load management, the system incorporates a liquid accumulator, model RICEV. FL 40.27+SGR7+2S89

(M54/M54) designed by Frigomec. The accumulator features 4 connections, 2 DN50 connected to the refrigerant cycle (inlet, outlet) and another 2 DN80 to add a differential pressure sensor, which acts as a refrigerant level sensor. This component is essential for storing excess refrigerant charge during transitions between operating modes, which typically differ between modes (Cendoya et al., 2024).

The expander operates at a constant speed of 50 Hz. However, an inverter is required to interface with the electrical grid, in compliance with Belgian regulations, which prohibit feeding electricity into the grid without a Synergrid-approved inverter. To meet this requirement, four 20 kVA Hercules inverter modules, supplied by CE+T Power, have been integrated into the system. The compressor is driven by a Bitzer FRW-240+4 frequency inverter, which allows operation between 30 Hz and 60 Hz to optimise the COP under different operating conditions. These systems are equipped with an internal oil circuit, which significantly reduces the amount of oil components required. In the case of the expander, only a single external lubrication kit is needed to monitor and ensure adequate equipment lubrication. This kit is directly connected to the oil inlet and outlet and does not require a separation and re-injection circuit. The refrigerant motor pump is equipped with an ODE-4-11kW frequency inverter from Invertek Drives, which is selected to achieve the various operating conditions of the refrigerant. For the water circuit, three centrifugal pumps Etabloc 065-050-125 GC from KSB have been selected, each equipped with its own PumpDrive 2 frequency drive from KSB. These pumps were chosen for their high efficiency and minimal performance loss when operating with a frequency drive (KSB Aktiengesellschaft, 2017). Additionally, they are capable of transporting large water flows at relatively low head heights.

The working fluid selected corresponds to R1233ZD(E), chosen for its low Global Warming Potential of 1, non-flammability and non-toxicity (Calvin et al., 2023). This refrigerant has been widely recommended for CB systems, due to its high efficiency (Fan & Xi, 2022). Moreover, this fluid offers a favourable compatibility with commercially available components, making it a practical choice for this application (Steger et al., 2020). The secondary fluid is water, chosen for its low cost and widespread availability at the study site. This refrigerant also presents significant challenges regarding chemical compatibility. According to the document “A Better Environment with Next-Generation Solstice®zd Refrigerant” from Honeywell (Honeywell, 2018), R1233zd(E) is incompatible with traditional EPDM seals, while classic Viton sealings are suitable only under certain conditions. On the other hand, Teflon and Neoprene present high compatibility, being the preferred sealing for this refrigerant. Therefore, the careful selection of system components is essential. In this case, both the expander and compressor are designed by the manufacturer to operate with this refrigerant, eliminating potential incompatibility issues. Special consideration must be given to the ORC pump, as incompatibility could lead to premature failure and a decrease in performance. Regarding valves in contact with the refrigerant, the use of Teflon seals is recommended to prevent leakage and ensure proper operation.

For the piping system, special attention is given to minimising pressure drops. For the liquid phase, velocity is maintained within the specified range of 1-3 m/s, while for the vapour phase, it remains within 10-20 m/s (Kast et al., 2010). The most critical location is at the expander exhaust and the condenser inlet, where the fluid's low density results in high velocities, elevated Reynolds numbers, and consequently significant pressure drops. These effects become particularly critical when operating at pressures lower than atmospheric. Additionally, on the refrigerant side, all materials are selected to be stainless steel to ensure compatibility and durability, while carbon steel is used for the waterside due to its cost-effectiveness and suitability for the application.

The data acquisition system consists of a CompactDAQ with eight slots from National Instruments. This device is used to read all control variables, including power consumption parameters. These variables are processed in real time through LabVIEW, where four different PID controllers regulate the system: Expansion valve opening to maintain a minimum superheating of 8 K in HP mode. Compressor speed to optimise the COP under varying operating conditions. The ORC pump speed varied to generate the optimal pressure differential for the expander operation. Water pump control is used to achieve the optimal glide of the secondary fluid, enhancing overall system performance.

## 5 NUMERICAL SIMULATION

The numerical design is implemented in Python, following a modular approach for modelling the different system components. Heat exchangers are discretised based on the different working fluid regions: subcooled, two-phase, and superheated (Cuevas et al., 2009). In these regions, heat transfer correlations, pressure drop calculations, and void fraction correlations are incorporated to enhance accuracy. For the expander and compressor, semi-empirical models are implemented (Lemort et al., 2009; Cuevas et al., 2010), accounting for leakage effects, fluid heating and cooling due to heat exchange with other masses (oil and metal) and the environment, as well as under- and over-compression/expansion phenomena and the electromechanical losses are considered. The pump model is developed by fitting power, pressure, and flow factors to manufacturer data, enabling accurate performance prediction under varying operational speeds (Eck, 1973). Piping effects are computed through the pressure drops related to the friction and fitting (Kast et al., 2010). Thermodynamic properties are obtained using the CoolProp library (Bell et al., 2014), while the iteration problem is solved using the Modified Powell method, available in the Scipy library (Virtanen et al., 2020). Several variables are used as iterations in both modes. Regarding the ORC, more details can be found in the study of Cendoya et al.(2024). The resume of the model integration is presented in Figure 3, where it is possible to see the main inputs and outputs of the CB. It is also important to note that several parameters must be provided, such as the geometry of the heat exchangers and the parameters for the compressor, expander, and pumps, obtained from the error minimisation process.

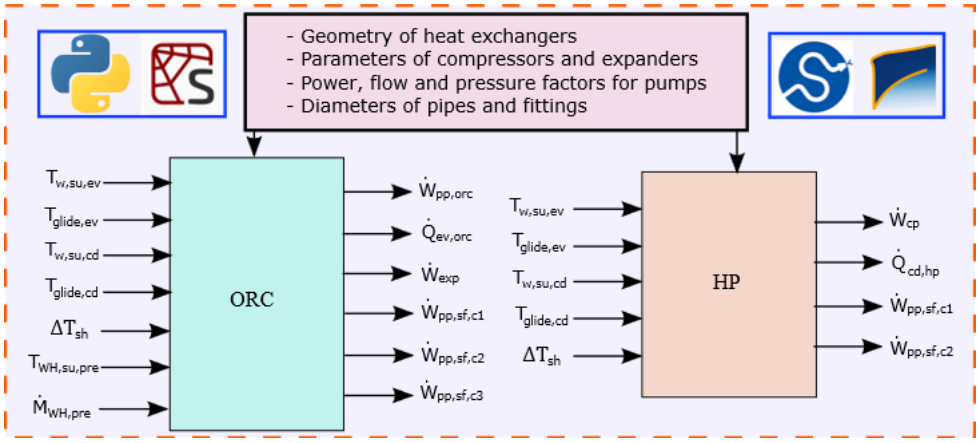


**Figure 3:** Resume of the main inputs, outputs and parameters for the modelling of the system

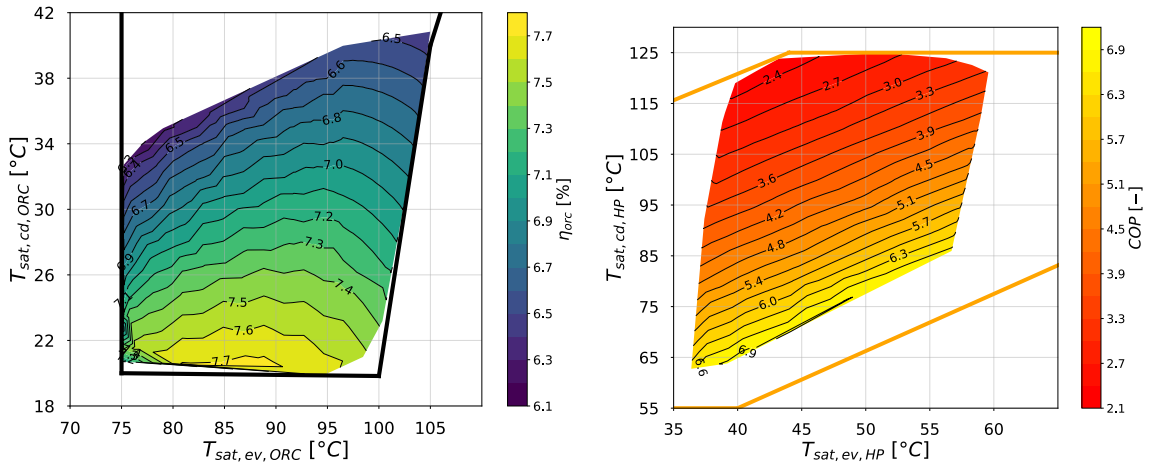


(a) (b)

**Figure 4:** Global performance of a) ORC mode and b) HP mode across different boundary conditions

After the design of the system, all the components' parameters are integrated into the modelling, allowing to obtain the performance of the system under part-load operation, as a result of different

secondary fluid conditions. Equation 1 is used to compute the ORC efficiency, while Equation 2 is used for the COP calculation. The results are presented in Figures 4a and 4b for the ORC and HP, respectively.

$$\eta_{orc} = \frac{\dot{W}_{exp} - \dot{W}_{pp,orc} - \sum \dot{W}_{pp,sf,i}}{\dot{Q}_{ev,orc}} \quad (1)$$

$$COP = \frac{\dot{Q}_{cd,hp}}{\dot{W}_{cp} + \sum \dot{W}_{pp,sf,i}} \quad (2)$$

Note that the performance of both modes takes into account all energy consumption of auxiliary components, such as water and refrigerant pumps. For the ORC and HP, a control strategy is chosen that keeps the best glide values at all conditions. These two plots are constrained by the operational envelope of the expander and compressor, which has been provided by the manufacturer. Additionally, the white space within the graph corresponds to points which are outside the operating conditions, and it does not make sense to run the entire simulation for all these points.

## 6 PROTOTYPE DEVELOPMENT

The global 3D model of the machine is illustrated in Figure 5, where the CB, as well as the different components and their circuits, can be appreciated. In addition, the dimension of the container, which will be used to transport it, is shown. The 3D was built in Autodesk Inventor 2025, and the component files were obtained from the different manufacturers, while the piping and its fittings were extracted from the available libraries.

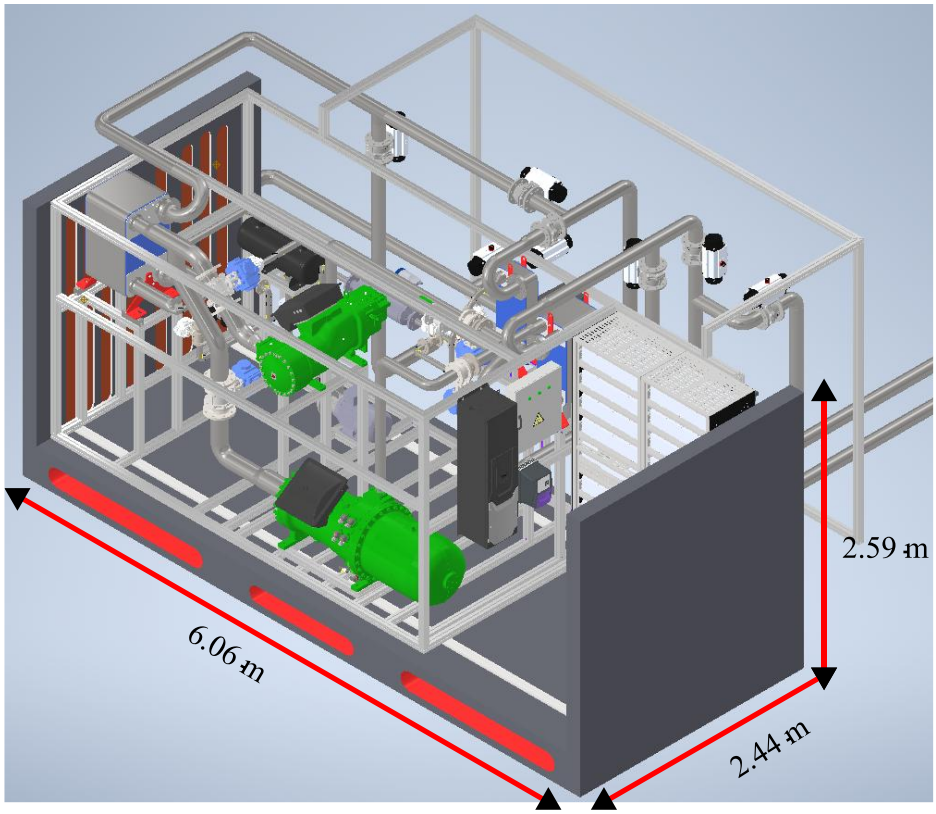


**Figure 5:** The 3D model of the CB, which is currently under development

## 7 CONCLUSION AND FUTURE WORK

This paper presents the design and component selection for CB, which shares nearly all components except for the expander and compressor. The prototype is designed to produce 50 kWe under ORC mode and 600 kWth in heat pump mode. In heat pump mode, the system is capable of reaching a

maximum saturation temperature of 125°C at the condenser, which generates a lot of interest for industrial and heating applications. A comprehensive numerical model has been developed which accurately predicts the system's operational performance under both modes, considering all relevant physical phenomena and auxiliary consumption. The machine is scheduled for commissioning in early 2026, with full testing expected by mid-2026 at the demonstration site. The results presented provide valuable insights into the design and component selection for both ORC and medium-to-high temperature HP systems. These insights are particularly relevant for applications in neighbourhoods, such as district heating and also in the transition to smart residential areas, able to self-produce their own energy. Moreover, for industries which use hot water or even saturated vapour for their process. The primary control variables have been identified and will be further validated through the upcoming operational campaign. The boundary conditions for the system will be dictated by the underground cavern's capabilities, with the charging period set to begin in the summer of 2025.

## NOMENCLATURE

| | | | | | |
|---|---|---|---|---|---|
| $A$ | Area | ($m^2$) | NPSH | Net Positive Suction Head | (-) |
| $CB$ | Carnot Battery | (-) | $ORC$ | Organic Rankine Cycle | (-) |
| $COP$ | Coefficient of Performance | (-) | $\dot{Q}$ | Heat Flow Rate | (kW) |
| HP | Heat Pump | (-) | $T$ | Temperature | (°C) |
| $\dot{M}$ | Mass Flow Rate | (kg/s) | $\dot{W}$ | Power | (kW) |
| **Greek letters** | | | | | |
| $\eta$ | Efficiency | (-) | $\Delta$ | Difference | (-) |
| **Subscript** | | | | | |
| c1 | circuit 1 | | nom | nominal | |
| c2 | circuit 2 | | pp | pump | |
| c3 | circuit 3 | | pre | preheater | |
| cd | condenser | | sat | saturation | |
| cp | compressor | | sf | secondary fluid | |
| ev | evaporator | | sh | superheating | |
| exp | expander | | su | supply | |
| glide | glide | | w | water | |
| i | number | | wh | waste heat | |

## REFERENCES


Bell, I. H., Wronski, J., Quoilin, S., & Lemort, V. (2014). Pure and Pseudo-pure Fluid Thermophysical Property Evaluation and the Open-Source Thermophysical Property Library CoolProp. *Ind. Eng. Chem. Res.*, **53**(6), 2498–2508. https://doi.org/10.1021/ie4033999

Cendoya, A., et al. (2024). Carnot Battery integration in a geothermal power plant: Study case of Zorlu Energy. *1st Belg. Symp. Thermodyn.*, Liège, Belgium.

Cendoya, A., et al. (2024). Numerical Modelling of a 50 kWe reversible Carnot Battery coupled with waste heat. *1st Belg. Symp. Thermodyn.*, Liège, Belgium.

Cendoya, A., et al. (2024). Modelling and Simulation of a Carnot Battery Coupled to Seasonal Underground Stratified Thermal Energy Storage for Heating, Cooling and Electricity Generation. *Int. High Perform. Build. Conf.*, **10**. https://docs.lib.purdue.edu/ihpbc/472/

Cuevas, C., et al. (2009). Development and validation of a condenser three zones model. *Appl. Therm. Eng.*, **29**(17–18), 3542–3551. https://doi.org/10.1016/j.applthermaleng.2009.06.007

Cuevas, C., et al. (2010). Characterization of a scroll compressor under extended operating conditions. *Appl. Therm. Eng.*, **30**(6–7), 605–615. https://doi.org/10.1016/j.applthermaleng.2009.11.005

Daniarta, S., et al. (2024). Performance map and theoretical analysis of Carnot battery technology via novel reversible Rankine-based cycle. *Energy Rep.*, **11**, 4500–4514. https://doi.org/10.1016/j.egyr.2024.04.024

Dumont, O. (2017). Investigation of a heat pump reversible in an organic Rankine cycle and its application in the building sector. https://orbi.uliege.be/handle/2268/218181

Dumont, O., et al. (2018). Experimental investigation and optimal performance assessment of four volumetric expanders (scroll, screw, piston and roots) tested in a small-scale organic Rankine cycle system. *Energy*, **165**, 1119–1127. https://doi.org/10.1016/j.energy.2018.06.182

Eck, B. (1973). *Fans: Design and Operation of Centrifugal, Axial-Flow and Cross-Flow Fans* (1st ed.). Pergamon Press.

Fan, R., & Xi, H. (2022). Exergoeconomic optimization and working fluid comparison of low-temperature Carnot battery systems for energy storage. *J. Energy Storage*, 51, 104453. https://doi.org/10.1016/j.est.2022.104453

Guo, B., Lemort, V., & Cendoya, A. (2025). Control strategy and techno-economic optimization of a small-scale hybrid energy storage system: Reversible HP/ORC-based Carnot battery and electrical battery. *Energy*, 329, 136508. https://doi.org/10.1016/j.energy.2025.136508

Honeywell. (2018). A Better Environment with Next-Generation Solstice® zd Refrigerant. *Honeywell*. https://www.honeywell-refrigerants.com/europe/wp-content/uploads/2018/11/Honeywell-Solstice-zd-Brochure_EN.pdf

Kast, W., Nirschl, H., & Gaddis, E. (2010). L1 pressure drop in single phase flow. In *VDI Heat Atlas* (2nd ed., pp. 1053–1116). https://link.springer.com/referenceworkentry/10.1007/978-3-540-77877-6_70

Kaufmann, F., et al. (2024). Experimental Analysis of a Reversible High-Temperature Heat Pump/Orc Test Rig for Geothermal CHP Applications. *SSRN*. https://doi.org/10.2139/ssrn.5013851

KSB Aktiengesellschaft. (2017). *KSB SuPremE® in IE5: The world's most efficient magnet-less pump motor*. https://www.ksb.com/en-be/lc/products/motor/ksb-supreme/SD8C

Lemort, V., et al. (2009). Testing and modeling a scroll expander integrated into an Organic Rankine Cycle. *Appl. Therm. Eng.*, **29**(14–15), 3094–3102. https://doi.org/10.1016/j.applthermaleng.2009.04.013

Ravindran, R. V., et al. (2024). Experimental investigation of a small-scale reversible high-temperature heat pump − organic Rankine cycle system. *Appl. Therm. Eng.*, **257**, 124237. https://doi.org/10.1016/j.applthermaleng.2024.124237

Steger, D., et al. (2020). Design aspects of a reversible heat pump—Organic rankine cycle pilot plant for energy storage. *Energy*, **208**, 118216. https://doi.org/10.1016/j.energy.2020.118216

Theologou, K., et al. (2024). CHESTER: Experimental prototype of a compressed heat energy storage and management system. *Energy Convers. Manag.*, **311**, 118519. https://doi.org/10.1016/j.enconman.2024.118519

Vecchi, A., et al. (2022). Carnot Battery development: A review on system performance, applications and commercial state-of-the-art. *J. Energy Storage*, **55**, 105782. https://doi.org/10.1016/j.est.2022.105782

Virtanen, P., et al. (2020). SciPy 1.0: Fundamental algorithms for scientific computing in Python. *Nat. Methods*, **17**(3), 261–272. https://doi.org/10.1038/s41592-019-0686-2

Weitzer, M., et al. (2024). Reversible heat pump—Organic Rankine Cycle systems with zeotropic fluid mixtures. *Int. Refrig. Air Cond. Conf.*, HERRICK 2024, West Lafayette, IN, USA. https://docs.lib.purdue.edu/iracc/2614/

Weitzer, M., Müller, D., & Karl, J. (2023). Reversible Heat Pump-ORC Pilot Plant – Experimental Results and Fluid Charge Optimization. In D. T. Sánchez Martínez (Ed.), *Proc. 7th Int. Semin. ORC Power Syst. (ORC 2023)* (pp. 430–438). Editorial Universidad de Sevilla. https://doi.org/10.12795/9788447227457_72

Xu, Z. Y., Wang, R. Z., & Yang, C. (2019). Perspectives for low-temperature waste heat recovery. *Energy*, **176**, 1037–1043. https://doi.org/10.1016/j.energy.2019.04.001

## ACKNOWLEDGEMENTS

The project that produced the results presented in this paper has received funding from the European Union's Horizon Research and Innovation programme under grant agreement No. 10112355, in the framework of the WeForming project. The authors would also like to acknowledge the funding provided by the Walloon Region of Belgium in the framework of the ARDNrgy project.